Comparing UAV-based multispectral indices with thermal and energy balance models for barley yield components estimation

David Gómez-Candón[1,2], Alejandra Cabeza[1], Dolors Villegas[1], Ana M. Casas[1], Ernesto Igartua[1]

[1]Aula Dei Experimental Station (EEAD-CSIC), 50080 Zaragoza, Spain
[2]ARAID Foundation, 50004 Zaragoza, Spain

Abstract.

Accurate estimation of barley yield components is essential for improving crop management and breeding strategies under contrasting water regimes. This study evaluates the potential of integrating unmanned aerial vehicle (UAV)-based multispectral and thermal imagery with energy balance modeling to predict grain yield (GY), thousand kernel weight (TKW), and grain filling period (GFP). A recombinant inbred line (RIL) population derived from SBCC073 × Cierzo was grown under irrigated and rainfed conditions in Spain during the 2019 season. UAV flights were conducted at two phenological stages—pre-flowering (March 22) and post-flowering (May 16)—to capture high-resolution multispectral and thermal data. Multispectral images were processed into reflectance orthomosaics, from which 18 vegetation indices (VIs) were computed, while thermal imagery supported the estimation of biophysical parameters such as evapotranspiration (ET) and transpiration (T) using the Two-Source Energy Balance (TSEB) model. Yield components exhibited strong treatment effects: irrigated plots achieved higher GY (5.76 t·ha^{-1}) and TKW (37.33 g) but shorter GFP (12.26 days) compared to rainfed plots (GY = 2.52 t·ha^{-1}; TKW = 30.63 g; GFP = 36.66 days). Broad-sense heritability was moderate-to-high for TKW (H^2 = 0.862 irrigated; 0.702 rainfed) and GFP (0.667; 0.678), but lower for GY under rainfed conditions (H^2 = 0.550), indicating strong environmental influence on yield stability. Correlation analysis revealed that ET and T were the most informative predictors for GY and TKW under rainfed conditions ($r \approx 0.65$–0.67), while post-flowering VIs such as NDVI, IPVI, and RDVI were most effective for GFP ($r \approx 0.62$–0.67). Under irrigation, VI signals tended to saturate, reducing their predictive power, whereas biophysical parameters retained moderate explanatory value for GY.

These findings underscore the advantages of the ET and T biophysical parameters for estimating yield components. They also support the use of UAV-based remote sensing combined with energy balance modeling for high-throughput phenotyping. Early-season measurements of ET and VIs offer valuable information for proactive crop management and genotype screening. Post-flowering VIs remain critical for phenological traits, such as GFP. Future research should focus on multi-year validation, integration of three-dimensional canopy traits, and genotype-specific adjustments to enhance the robustness and scalability of breeding programs targeting drought resilience and grain quality.

This work has been carried out within the framework of projects AGL2016-80967-R, funded by MINECO/AEI and FEDER, PID2022-142116OB-I00, funded by MCIN/AEI and Project PID2023-

149687OR-C32, funded by MICIU/AEI/10.13039/501100011033/ and by FEDER, EU.

Keywords.
Unmanned Aerial Vehicles, Energy balance model, Barley Yield, thousand kernel weight, grain filling period

1. Introduction

The integration of remote sensing technologies, particularly unmanned aerial vehicles (UAVs) equipped with multispectral and thermal cameras, has revolutionized agricultural research and precision farming. These tools enable non-destructive, rapid, and accurate data collection across large areas, significantly improving crop monitoring and trait evaluation (Berni et al., 2009). Multispectral imaging captures reflectance at specific wavelengths, such as those in the visible (400–700 nm) and near-infrared (700–1100 nm) ranges, which are sensitive to plant physiological states. Vegetation indices (VIs) derived from this reflectance, including the Normalized Difference Vegetation Index (NDVI), Green Normalized Difference Vegetation Index (GNDVI), Ratio Vegetation Index (RVI), and Green Vegetation Index (GVI), are widely used to monitor key plant traits such as biomass, leaf area, and photosynthetic efficiency (Gracia-Romero et al., 2023). These indices provide critical insights into crop health, offering a means to assess chlorophyll content, water stress, and growth dynamics. Remote images and multispectral indices are instrumental in estimating plant biomass throughout growth stages, which is a critical yield indicator (Gómez-Candón et al., 2023). For instance, NDVI has been extensively applied to estimate biomass, an essential yield predictor, at various phenological stages (Näsi et al., 2018; Herzig et al., 2021). Such applications enable informed decision-making in crop management, including optimizing irrigation and fertilization strategies to enhance yield (Kefauver et al., 2017).

In addition to multispectral imaging, UAV-based thermal imaging has proven effective for assessing water stress, a major factor affecting crop performance (Messina and Modica, 2020). The thermal energy balance models, such as the Two-Source Energy Balance (TSEB) model, have been particularly valuable for estimating transpiration (T) and evapotranspiration (ET) (Norman et al., 1995; Kustas and Anderson, 2009). These physiological parameters are robust indicators of crop water use and productivity, providing a complementary perspective to vegetation indices in evaluating yield components. Applying energy balance models combined with UAV-based multispectral and thermal imaging to phenotyping platforms has shown great potential for precision agriculture and agronomic research (Gómez-Candón et al, 2021).

In Spain, barley cultivars are widely distributed across the country, particularly in agro-climatic regions with water scarcity (Matinez-Moreno et al., 2024). To obtain new varieties adapted to these regions, the Spanish Barley Core Collection (SBCC) is a valuable resource for breeding in the Mediterranean region, using the adaptive potential of Spanish landraces. (Igartua et al., 1998).

The aim of this study was to evaluate the potential of integrating VIs and physiological parameters, such as T and ET, derived from UAV-based imaging, for estimating key yield components in barley, including grain yield (GY), thousand kernel weight (TKW), and grain filling period (GFP). It was explored also the utility of ML models to determine the most relevant remote sensing variables, identify optimal combinations for yield components, and assess the accuracy of these models at different phenological stages.

2. Material and methods

2.1. Plant material, study site and experimental design

Our study was conducted on a barley high-throughput field phenotyping platform established at two distinct sites in Spain, representing contrasting water treatments. The irrigated site, Aula Dei (41º43’41’’N, 0º48’40’’ W), and the rainfed site, Vedado (41º46’16’’N, 0º43’31’’ W), were used to assess the yield components of 96 recombinant inbred line (RIL) population. This barley BC2F5 population derived from a cross between the six-rowed barley varieties SBCC073 and Cierzo. SBCC073 is a landrace from the SBCC, with acceptable agronomic performance despite being lodging-prone (Yahiaoui et al., 2014). Cierzo is an elite barley cultivar resulting from the cross Orria × Plaisant, characterized by its high yield performance and medium-to-tall height. The cross of SBCC073 and Cierzo have been genotyped and studied under field conditions before (Monteagudo et al., 2019).

Orria and Peweter were used as check varieties in Aula Dei while Ketos and Fidericus were in Vedado. Field plots were established under randomized block designs with two replicates per genotype at each site (200 plots per location). Each plot consisted of four rows that were 3.0m long x 0.8m wide. Figure 1 illustrates the geographic locations and layouts of both study sites, Aula Dei and Vedado, denoted as irrigated and rainfed conditions, respectively.

The yield components assessed include were the Grain Filling Period (GFP, Julian days), Grain Yield (GY, $t \cdot ha^{-1}$) and Thousand Kernel Weight (TKW, g). The GFP represents the active grain development period, it was calculated by subtracting maturity date obtained by NDVI value (using Greenseeker® portable device) and the awn tipping date, in Julian days both. The GY which quantifies productivity and TKW which indicates kernel weight and grain quality were assessed after harvest.

Figure 1. Location of study sites Aula Dei and Vedado (marked in blue).

2.2. UAV flights and vegetation indices

In 2019, UAV-based remote image data collection was conducted at both study sites (Aula Dei, irrigated, and Vedado, rainfed) through two flights: a pre-flowering flight on March 22 and a post-flowering flight on May 16. Thermal images were captured using an Ebee X UAV equipped with a Duet T thermal camera (Sensefly®, Switzerland) (Figure 2A). Multispectral images were captured with a Parrot Bluegrass Fields UAV, equipped with a Parrot Sequoia camera (ParrotDrone SAS, Paris, France) (Figure 2B). The Parrot Sequoia camera acquired data in four spectral bands: green (G, 550±40 nm), red (R, 660±40 nm), red edge (RE, 735±10 nm), and near-infrared (NIR, 790±40 nm). The UAV flights were conducted at 90 m altitude under sunny, low-wind conditions (≤12 m/s) around solar noon (~12:00 h) to minimize light variation. Forward and side overlaps were configured to 75% and 80%, respectively, ensuring optimal coverage and image quality.

Figure 2. UAVs and sensors used in the study. A. Duet T thermal camera (left) and Ebee X fixed wing UAV (right). B. Parrot Sequoia multispectral sensor (left) and Parrot Bluegrass Fields multirotor UAV (right).

Post-flight image processing was conducted with Pix4Dmapper Pro (version 4.3 – Pix4D SA, Switzerland), where images were aligned, ortho-mosaicked, and radiometrically corrected. Reflectance values were calibrated using a grey reference panel placed in the field. Resulted spatial resolution (Ground Sampling Distance, GSD) of generated reflectance ortho-mosaics was 0.02 m per multispectral band and 0.10 m for the thermal data. For subsequent analyses, only the areas occupied by plots were considered, excluding surrounding bare soil to focus solely on crop data.

Table 1. Chosen canopy reflectance vegetation indices. NIR: Near Infrared.

Index	Acronym	Equation	Authors
Normalized Difference VI	NDVI	$\frac{NIR - Red}{NIR + Red}$	Sellers, 1985
Green Normalized Difference VI	GNDVI	$\frac{NIR - Green}{NIR + Green}$	Ma et al., 1996
Red Ratio VI	RVI	$\frac{NIR}{Red}$	Rirth and McVey, 1968
Green Ratio VI	GVI	$\frac{NIR}{Green}$	Birth and McVey, 1968
Difference VI	DVI	$NIR - Red$	Perry and Lautenschlager, 1984
Greenness Index	GI	$\frac{Green}{Red}$	Smith et al., 1995
Green Red VI	GRVI	$\frac{Green - Red}{Green + Red}$	Tucker, 1979
Chlorophyll index Green	CIgreen	$\frac{NIR}{Green - 1}$	Gitelson et al., 2003
Chlorophyll Index - Red-Edge	CIre	$\frac{NIR}{Red\ Edge} - 1$	Gitelson et al., 2005
Infrarede Percentage VI	IPVI	$\frac{NIR}{NIR - Red}$	Panek et al., 2020
Normalized Difference red Edge index	NDRE	$\frac{NIR - Red\ Edge}{NIR + Red\ Edge}$	Fitgerald et al., 2006
Renormailzed Difference VI	RDVI	$\frac{NIR - Red}{\sqrt{NIR + Red}}$	Roujean and Breon, 1995
Modified Simple Ratio red edge	MSR	$\frac{NIR/(Red - 1)}{\sqrt{NIR/Red + 1}}$	Sun et al., 2022
Soil Adjusted VI	SAVI	$(1 + 0{,}5)\frac{NIR - Red}{NIR + Red + 0{,}5}$	Huete, 1988
Optimized soil Adjusted VI	OSAVI	$\frac{1.5NIR - Red}{NIR + Red + 0.16}$	Rondeaux et al., 1996
Modified Soil Adjusted VI	MSAVI	$\frac{2NIR + 1 - \sqrt{(NIR + 1)^2 - 8(NIR - Red)}}{2}$	Qi et al., 1994
Modified Chlorophyll Absorption in Reflectance Index	MCARI	$\frac{[(RedEdge - Red) - 0.2(RedEdge - Green)]Red}{Red}$	Daughtry et al., 2000
Transformed VI	TVI	$0.5(120(RedEdge - Green) - 200(Red - Green))$	Broge and Leblanc, 2001

In order to monitor yield components, eighteen vegetation indices (VIs) known for their efficacy in predicting crop characteristics were calculated by combining different reflectance bands (Table 1). The average value of each index was computed for individual plots using QGIS software and afterwards extracted. The VIs used in this study were selected based on their relevance to key physiological and structural traits of barley. They were grouped into four functional categories: (i) Greenness and biomass indicators, including NDVI, GNDVI, RVI, GVI, RDVI, and OSAVI, which are commonly used to estimate canopy vigor, leaf area, and overall biomass; (ii) Chlorophyll and pigment-sensitive indices, such as CIgreen, CIre, NDRE, MCARI, and MTCI, which are designed to capture variations in chlorophyll content and photosynthetic activity, particularly useful for detecting stress and senescence; (iii) Structural and geometric indices, including TVI, MTVI, and TCI, which provide information on canopy architecture and light interception; and (iv) Soil-adjusted indices, such as SAVI, MSAVI, and OSAVI, which correct for soil background effects and are particularly useful in early growth stages or sparse canopies.

2.3. Crop Evapotranspiration and Transpiration

The biophysical traits Actual ET and T values were estimated on each image acquisition date using the Two-Source Energy Balance (TSEB) model (Norman et al., 1995; Kustas and Anderson, 2009), which partitions surface energy fluxes between nominal soil and canopy sources. This partitioning allows for a more accurate assessment of soil and crop water dynamics under different environmental conditions. In this study, both soil temperature and canopy temperature were derived from the high-resolution thermal images (Nieto et al., 2019). In addition to surface temperatures, the TSEB model requires meteorological and biophysical inputs, including plant height (PH), leaf area index (LAI), and canopy cover fraction (fc) which were estimated following the methodology proposed by Gómez-Candón et al (2021). Meteorological data, including air temperature, wind speed, and relative humidity, was obtained from a nearby weather station belonging to the Spanish Agroclimatic Information System for Irrigation (SIAR, www.siar.es). These data inputs enabled the accurate computation of energy fluxes associated with each component.

The Python script used to implement TSEB for this study is available online at https://github.com/hectornieto/pyTSEB (last accessed 22 October 2025). This tool provides reproducibility and transparency for the methodological approach used to estimate evapotranspiration and transpiration in this study.

2.5. Statistical analysis

Mixed models were calculated for each trait (GY, TKW, and GFP) by treatment (Irrigated and Rainfed separately), with genotype as a random effect and a fixed intercept. Broad-sense Heritability was estimated from the variance components $\delta_g{}^2$ (genotype) and $\delta_e{}^2$ (residual).

$$H^2 = \frac{\delta_g^2}{\delta_g^2 + {\delta_e^2}/{r}} ,$$

where r = 2 replicates per genotype and treatment. This model was fitted to all plots in the corresponding treatment.

Additionally, a two-way exploratory ANOVA (treatment by genotype) was performed on the unique values of yield component per plot to verify the magnitude of the treatment effect.

Thus, for each date (pre-flowering and post-flowering), a matrix was constructed with 18 VIs. The columns were standardized using the z-score method, and Principal Component Analysis (PCA) was applied. The variance explained by the first components and the principal loadings were reported to interpret the axes.

To assess biophysical traits and VIs performance to predict yield components, Pearson correlations were calculated between each predictor (VIs and biophysical traits) and each yield component (GY, TKW, and GFP) for each treatment and date (pre-flowering and post-flowering). To facilitate discussion, the six to eight associations with the highest absolute r-values in each case are listed and the p-values were shown.

3. Results and discussion

This study was conducted using UAV imagery from only two phenological stages (pre-flowering and post-flowering), which may limit the temporal resolution of trait dynamics. Additionally, spatial effects such as micro-environmental variability within plots were not explicitly modeled, which could influence trait expression and remote sensing signals. Future studies should consider multi-temporal acquisitions and spatial modeling to enhance robustness

3.1. Yield components

Significant differences were observed in GY (t·ha^{-1}) between irrigated and rainfed conditions. The mean GY under irrigation was 5.76 t·ha^{-1}, markedly higher than the 2.52 t·ha^{-1} observed under rainfed conditions. Variability in GY was slightly greater under irrigation (standard deviation of 0.70) compared to rainfed (0.56), potentially reflecting greater sensitivity of yield to environmental or management factors under well-watered conditions (Figure 3A).

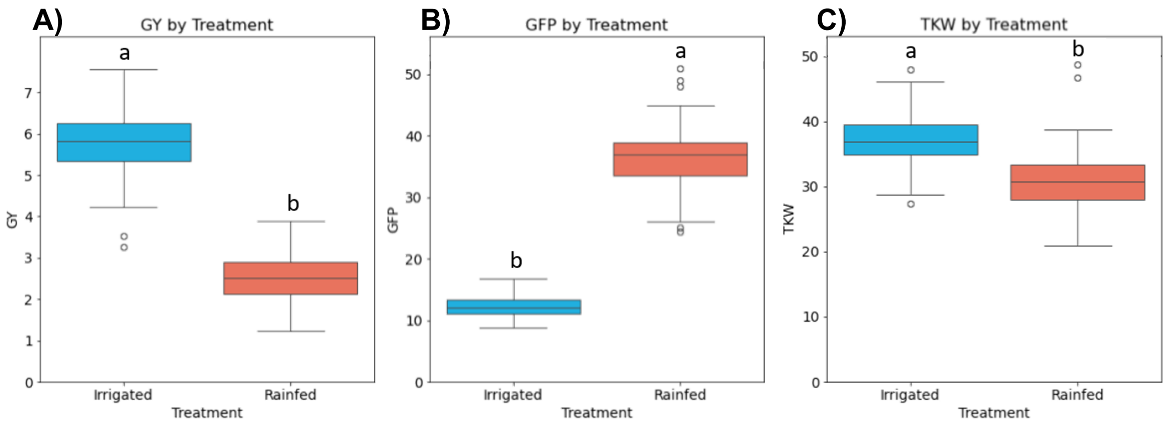

Figure 3. Influence of irrigation treatment (irrigated and rainfed) on yield components: A) Grain Yield (GY, t·ha^{-1}), B) Grain Filling Period (GFP, Julian days), and C) Thousand Kernel Weight (TKW, g). Circles represent extreme outliers. Different letters indicate significant differences between nitrogen treatments at the same temperature assuming a significance level of alpha = 0.05, using Duncan's fair significant difference test.

An exploratory ANOVA (treatment × genotype) for GY showed very significant effects: Treatment (p 10^{-126}), Genotype (p 0.0016), and Treatment × Genotype (p 0.022). This suggests detectable Genotype × Environment interactions. The main analysis, however, is presented by treatment.

On the other hand, the grain GFP was substantially longer under rainfed conditions, likely due to the advantage of early flowering genotypes that capitalize on residual soil moisture. This phenological shift suggests an adaptive strategy to water-limited environments. GFP was considerably shorter under irrigation, with a mean duration of 12.26 days, compared to 36.66 days under rainfed conditions (Figure 3B). Awn tipping date under irrigated conditions occurred 36 Julian days later than in rainfed conditions and maturity date did only 12 Julian days later (data not shown). This different behavior under distinct irrigation regimens can be attributed to the advantage of earlier flowering RILs in rainfed conditions. Optimizing flowering time enables plants to take advantage of early rainfall and improved conditions for grain filling period.

Thus, TKW was also significantly higher under irrigation, averaging 37.33 g compared to 30.63 g under rainfed conditions (Figure 3C). This suggests that irrigation not only supports greater vegetative biomass but also promotes improved grain filling and kernel development.

These findings underscore the profound impact of water availability on yield components. While irrigation enhances GY and TKW, it shortens GFP, likely due to the expedited physiological processes enabled by consistent water supply. Yield components results confirm a strong treatment effect and a change in the phenological regime (higher GFP in Rainfed), which is consistent with rainfed conditions that lengthen the effective filling period measured under this scheme.

Table 2. Heritability by trait and treatment

Trait	Treatment	Genotype	Environment	H^2
Yield	Irrigated	0.274	0.215	0.717
TKW	Irrigated	8.541	2.740	0.862
GFP	Irrigated	1.290	1.288	0.667
Yield	Rainfed	0.119	0.195	0.550
TKW	Rainfed	10.131	8.579	0.702
GFP	Rainfed	9.653	9.184	0.678

Heritability estimates (H^2, Table 2) revealed moderate-to-high genetic consistency for TKW (0.862 and 0.702 for irrigated and rainfed respectively) and GFP (0.667 and 0.678 for irrigated and rainfed respectively) across treatments, indicating their suitability for selection. In contrast, GY under rainfed conditions showed lower heritability (H^2 of 0.550), highlighting the influence of environmental variability and the need for robust phenotyping strategies. These results support the use of treatment-specific models, validated by genotype, to estimate the value of unseen genotypes. In practice, this approach can be used to select materials that combine stability and suitability for each water condition. The randomized block design and genotype-stratified analysis enabled the detection of genotype × environment interactions, which are critical for breeding programs targeting drought resilience.

3.2. Vegetation Indices and physiological variables as barley yield estimators

This study was based on images acquired onboard UAVs, whose effectiveness in providing fast and reliable information from a large number of plots within barley crops has been demonstrated in numerous studies (Oehlschläger et al., 2018; Jafari et al., 2016). Principal Component Analysis (PCA) revealed that PC1 captured a vigor/biomass gradient (NDVI, RDVI, RVI, OSAVI), while PC2 was dominated by chlorophyll-sensitive indices (NDRE, CIre, MTCI), particularly informative during post-flowering stages. Indices such as NDRE and CIre are valuable for detecting stress responses and senescence, complementing vigor-based indices.

Table 3. Principal Component Analysis by date

Date	PC1	PC2	PC3
Pre-flowering	0.827	0.114	0.041
Post-flowering	0.924	0.050	0.014

From the PCA analysis results on VIs showed that PC1 explained ~82.7% and ~92.4% of the variance in the pre-flowering and post-flowering, respectively, while PC2 added ~11.4% and ~5.0%, respectively (Table 3). The loadings indicate that PC1 summarizes a vigor/greenness gradient (classic VIs, such as NDVI, RDVI, RVI, and OSAVI/MSAVI), while PC2 loads high on NDRE, MTCI, and CIre (sensitive to chlorophyll and red-edge), Figure 4. The TCARI/MTVI/TCI signal appears in secondary components associated with geometry, structure, and pigments. The correlation of PC1 scores with yield was moderate and treatment-dependent (arbitrary sign due to PCA indeterminacy) and lower for PC2. In particular, NDRE was particularly useful in capturing threshold-like behavior in chlorophyll content, especially under rainfed conditions. Its sensitivity to red-edge reflectance makes it a valuable indicator of physiological stress and senescence.

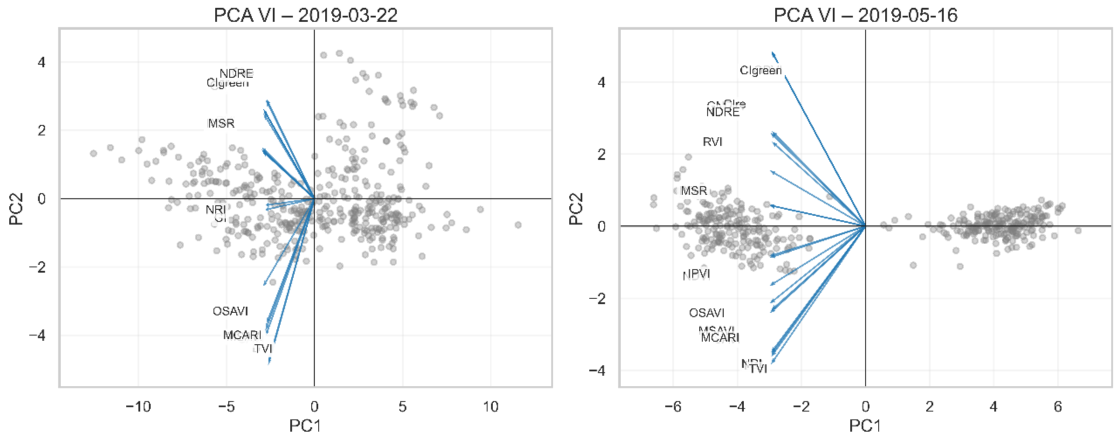

Figure 4. PCA biplots for pre- and post-processing. The NDRE, MTCI, and CIre vectors define PC2, while the vigor VI defines PC1.

Regarding to collinearity and latent axes, PC1 explained most of the variance (≥80%) and acted as a proxy for vigor/biomass, while PC2 captured chlorophyll/red edge (NDRE, MTCI, and CIre). This decomposition helps avoid multicollinearity in models and interpret the underlying physiological processes in each treatment. The correlation of PC1 with the traits varies in sign due to the indeterminacy of PCA, but the magnitude confirms that a single axis captures most of the VI information.

Physiological variables (ET and T) showed strong correlations with GY and TKW under rainfed conditions, underscoring the role of transpiration efficiency in yield maintenance. In irrigated environments, VIs tended to saturate, reducing their predictive power, while ET retained moderate explanatory value. Notably, post-flowering VIs were most informative for GFP, especially under rainfed conditions, where NDVI, IPVI, and RDVI reached $r \approx 0.67$.

The ability of pre-flowering ET and VIs to predict GY and GFP supports the use of early-season UAV flights for proactive crop management and genotype screening. These findings highlight the complementary nature of physiological and spectral data in yield estimation.

Regarding to biophysical estimations, ET and T, as suggested by Herzig et al (2021), VIs by itself become more informative as the season progresses. However, the results suggest that physiological variables (ET and T) are more reliable for early yield estimation. Importantly, the ability to achieve comparable predictive accuracy for GY and GFP at both phenological stages highlights the potential of early-season predictions to inform crop management decisions.

The treatment is the main differencing factor of the remote sensed data. Contrasts between Irrigated and Rainfed reveal significant variations in yield, TKW, and GFP. In Rainfed, the biophysical estimates (T or ET) dominate the associations with yield and TKW. This reflects water limitation and the role of transpiration in sustaining grain filling. Post-flowering VIs better explain GFP. In Irrigated treatment, variations in vigor are present, but ET and T retains more explanatory power for yield, with weaker associations for TKW and GFP. These patterns are as expected. Under rainfed conditions, transpiration related estimates better capture performance. Under irrigation, however, biomass and photosynthetic activity tend to saturate indices such as NDVI.

To assess biophysical traits and VIs performance to predict yield components, Pearson correlations (r-Pearson) were calculated between each predictor (VIs and biophysical traits) and each yield component (GY, TKW, and GFP) for each treatment and date (pre-flowering and post-flowering). To facilitate discussion, the six to eight associations with the highest absolute r-values in each case are listed and the p-values were shown.

For the GY, strong associations were found with T ($r = 0.67$), NDVI ($r = 0.65$), and GI, RVI, RDVI, and MSR ($r = 0.67 \pm 0.02$) in rainfed treatment and pre-flowering period. On the other hand, the better correlations were found for the T and ET block ($r = 0.65$) in post-flowering rainfed plants. Regarding to the irrigated treatment, moderate associations were found with ET and T (0.40–

0.47) and VIs contributed less (0.31–0.40).

For the TKW component, rainfed treatment T and ET (~0.43–0.48, post-flowering), and VIs of vigor and structure (GI) (~0.42–0.43, post-flowering). On the other hand, weak-moderate associations (|r| ≤ 0.25) with T and ET post-flowering in irrigated treatment.

Finally, there were found for the GFP component VIs (NDVI, IPVI, RDVI, RVI, OSAVI) with r ≈ 0.62–0.67 in rainfed post-flowering. Furthermore, in irrigated pre-flowering, low-moderate positive correlations with NDVI, GNDVI and IPVI (~0.27–0.29) and negative correlations with TCARI (~−0.30). In the post stage, the associations decrease (TCI: −0.29; the rest: <0.23).

4. Conclusion

This study demonstrates the potential of integrating UAV-based multispectral and thermal imagery with energy balance modeling and machine learning to estimate key barley yield components—grain yield (GY), thousand kernel weight (TKW), and grain filling period (GFP)—under contrasting water regimes. Physiological variables derived from the TSEB model (ET and T) consistently outperformed vegetation indices for predicting GY and TKW in rainfed environments, highlighting their relevance in water-limited conditions. Conversely, post-flowering vegetation indices proved most effective for GFP estimation, particularly under irrigation.

Acknowledgments

This work has been carried out within the framework of projects AGL2016-80967-R, funded by MINECO/AEI and FEDER, PID2022-142116OB-I00, funded by MCIN/AEI and Project PID2023-149687OR-C32, funded by MICIU/AEI/10.13039/501100011033/ and by FEDER, EU.

References

Berni, J. A., Zarco-Tejada, P. J., Suárez, L., & Fereres, E. (2009). Thermal and narrowband multispectral remote sensing for vegetation monitoring from an unmanned aerial vehicle. IEEE Transactions on geoscience and Remote Sensing, 47(3), 722-738.

Birth, G.S.; McVey, G.R. Measuring the color of growing turf with a reflectance spectrophotometer. Agron. J. 1968, 60, 640–643

Broge, N. H., & Leblanc, E. (2001). Comparing prediction power and stability of broadband and hyperspectral vegetation indices for estimation of green leaf area index and canopy chlorophyll density. Remote Sensing of Environment, 76(2), 156–172. https://doi.org/10. 1016/S0034-4257(00)00197-8

Daughtry, C. S., Walthall, C. L., Kim, M. S., Brown de Colstoun, E., and McMurtrey, J. E. (2000). Estimating corn leaf chlorophyll concentration from leaf and canopy reflectance. Remote Sens. Environ. 74, 229–239. doi: 10.1016/S0034-4257(00)00113-9

Fitzgerald, G. J., Rodriguez, D., Christensen, L. K., Belford, R., Sadras, V. O., & Clarke, T. R. (2006). Spectral and thermal sensing for nitrogen and water status in rainfed and irrigated wheat environments. Precision Agriculture, 7, 233–248

Gitelson, A.A.; Kaufman, Y.J.; Merzlyak, M.N. Use of a green channel in remote sensing of global vegetation from EOS-MODIS. Remote Sens. Environ. 1996, 58, 289–298

Gitelson, A. A., Gri, Y., & Merzlyak, M. N. (2003). Relationships between leaf chlorophyll content and spectral reflectance and algorithms for non-destructive chlorophyll assessment in higher plant leaves. Journal of Plant Physiology, 160(3), 271–282. https://doi.org/https://doi.org/10.1078/0176-1617-00887

Gitelson, A. A., Viña, A., Ciganda, V., Rundquist, D. C., Arkebauer, T. J. (2005). Remote estimation of canopy chlorophyll content in crops. Geophysical research letters, 32(8), 1-4.

Gómez-Candón, D., Bellvert, J., Royo, C. (2021). Performance of the two-source energy balance (TSEB) model as a tool for monitoring the response of durum wheat to drought by high-throughput field phenotyping. Frontiers in plant science, 12, 658357

Gómez-Candón, D.; Bellvert, J.; Pelechá, A.; Lopes, M.S. A Remote Sensing Approach for Assessing Daily Cumulative Evapotranspiration Integral in Wheat Genotype Screening for Drought Adaptation. Plants 2023, 12, 3871. https://doi.org/10.3390/plants12223871

Gracia-Romero A, Rufo R, Gómez-Candón D, Soriano JM, Bellvert J, Yannam VRR, Gulino D., Lopes MS (2023) Improving in-season wheat yield prediction using remote sensing and additional agronomic traits as predictors. Front. Plant Sci. 14:1063983. doi: 10.3389/fpls.2023.1063983

Haboudane,D., Miller, J. R., Pattey, E., Zarco-Tejada, P. J.,&Strachan, I. B. (2004). Hyperspectral vegetation indices and novel algorithms for predicting green LAI of crop canopies: Modeling and validation in the context of precision agriculture. Remote Sensing of Environment, 90(3), 337–352

Herzig, P.; Borrmann, P.; Knauer, U.; Klück, H.-C.; Kilias, D.; Seiffert, U.; Pillen, K.; Maurer, A. Evaluation of RGB and Multispectral Unmanned Aerial Vehicle (UAV) Imagery for High-Throughput Phenotyping and Yield Prediction in Barley Breeding. Remote Sens. 2021, 13, 2670. https://doi.org/10.3390/rs13142670

Huete, A. R. (1988). A soil-adjusted vegetation index (SAVI). Remote Sens. Environ. 25, 295–309. doi: 10.1016/0034-4257(88)90106-X

Igartua, E., Gracia, M. P., Lasa, J. M., Medina, B., Molina-Cano, J. L., Montoya, J. L., & Romagosa, I. (1998). The Spanish barley core collection. Genetic Resources and Crop Evolution, 45, 475-481.

Jafari, A., Werner, A., Fourie, J., & Hedley, C. (2016). Using multispectral imaging for indicating the water status of barley.

Jiang, Z.Y.; Huete, A.R.; Didan, K.; Miura, T. Development of a two-band enhanced vegetation index without a blue band. Remote Sens. Environ. 2008, 112, 3833–3845

Kefauver, S. C., Vicente, R., Vergara-Díaz, O., Fernandez-Gallego, J. A., Kerfal, S., Lopez, A., ... & Araus, J. L. (2017). Comparative UAV and field phenotyping to assess yield and nitrogen use efficiency in hybrid and conventional barley. Frontiers in Plant Science, 8, 1733.

Kustas, W.; Anderson, M. Advances in thermal infrared remote sensing for land surface modeling. Agric. For. Meteorol. 2009, 149, 2071–2081

Ma, B.L.; Morrison, M.J.; Dwyer, L.M. Canopy light reflectance and field greenness to assess nitrogen fertilization and yield of maize. Agron. J. 1996, 88, 915–920

Martínez-Moreno, F., Solís, I., & Igartua, E. (2024). Barley History and Breeding in Spain. Agriculture, 14(10), 1674.

Messina, G., & Modica, G. (2020). Applications of UAV thermal imagery in precision agriculture: State of the art and future research outlook. Remote Sensing, 12(9), 1491.

Messina, G., Badagliacca, G., Praticò, S., Preiti, G., Monti, M., & Modica, G. (2022). Multispectral UAV-Based Monitoring of Behavior of Different Wheat and Barley Varieties. In Conference of the Italian Society of Agricultural Engineering (pp. 1173-1181). Cham: Springer International Publishing.

Monteagudo, A., Casas, A. M., Cantalapiedra, C. P., Contreras-Moreira, B., Gracia, M. P., & Igartua, E. (2019). Harnessing novel diversity from landraces to improve an elite barley variety. Frontiers in Plant Science, 10, 434.

Nieto, H.; Kustas,W.P.; Torres-Rúa, A.; Alfieri, J.G.; Gao, F.; Anderson, M.C.; McKee, L.G. Evaluation of TSEB turbulent fluxes using different methods for the retrieval of soil and canopy component temperatures from UAV thermal and multispectral imagery. Irrig. Sci. 2019, 37, 389–406

Norman, J.M.; Kustas, W.P.; Humes, K.S. Source approach for estimating soil and vegetation energy fluxes in observations of directional radiometric surface temperature. Agric. For. Meteorol. 1995, 77, 263–293

Oehlschläger, J., Schmidhalter, U., & Noack, P. O. (2018, September). UAV-based hyperspectral sensing for yield prediction in winter barley. In 2018 9th Workshop on Hyperspectral Image and Signal Processing: Evolution in Remote Sensing (WHISPERS) (pp. 1-4). IEEE.

Panek, E., Gozdowski, D., Stępie´n, M., et al., 2020. Within-field relationships between satellite-derived vegetation indices, grain yield and spike number of winter wheat and triticale. Agronomy 10 (11), 1842

Perry, C. R., & Lautenschlager, L. F. (1984). Functional equivalence of spectral vegetation indices. Remote Sensing of Environment, 14(1–3), 169–182. https://doi.org/10.1016/0034-4257(84)90013-0

Pu, R., & Gong, P. (2011). Hyperspectral remote sensing of vegetation bioparameters. Advances in Environmental Remote Sensing: Sensors, Algorithms, and Applications, 7, 101–142

Qi, J., Chehbouni, A., Huete, A. R., Kerr, Y. H., & Sorooshian, S. (1994). A modified soil adjusted vegetation index. Remote Sensing of Environment, 48(2), 119–126. https://doi.org/10.1016/0034-4257(94)90134-1

Rondeaux, G., Steven, M., and Baret, F. (1996). Optimization of soiladjusted vegetation indices. Remote Sens. Environ. 55, 95–107. doi: 10.1016/0034-4257(95)00186-7

Roujean, J. L., and Breon, F. M. (1995). Estimating PAR absorbed by vegetation from bidirectional reflectance measurements. Remote Sens. Environ. 51, 375–384. doi: 10.1016/0034-4257(94)00114-3

Rouse, J. W., Haas, R. H., Schell, J. A., Deering, D. W., and Harlan, J. C. (1974). Monitoring the Vernal Advancements and Retrogradation of Natural Vegetation. Final Report, NASA/GSFC, Greenbelt, MD

Sellers, P.J. Canopy reflectance, photosynthesis and transpiration. Int. J. Remote Sens. 1985, 6, 1335–1372

Smith, R. C. G., Adams, J., Stephens, D. J., & Hick, P. T. (1995). Forecasting wheat yield in a Mediterranean-type environment from the NOAA satellite. Australian Journal of Agricultural Research, 46(1), 113–125

Sun, Q., Chen, L., Xu, X., et al., 2022. A new comprehensive index for monitoring maize lodging severity using UAV-based multi-spectral imagery. Comput. Electron. Agric. 202, 107362

Tucker, C.J. Red and photographic infrared linear combinations for monitoring vegetation. Remote Sens. Environ. 1979, 8, 127–150

Vincini, M., Frazzi, E., & D'Alessio, P. (2006, September). Angular dependence of maize and sugar beet VIs from directional CHRIS/Proba data. In Proceedings of the 4th ESA CHRIS PROBA Workshop (Vol. 2006, pp. 19–21). European Space Agency

Yahiaoui, S., Cuesta-Marcos, A., Gracia, M. P., Medina, B., Lasa, J. M., Casas, A. M., ... & Igartua, E. (2014). Spanish barley landraces outperform modern cultivars at low-productivity sites. Plant breeding, 133(2), 218-226.

Zhang, B., Gu, L., Dai, M., Bao, X., Sun, Q., Qu, X., ... & Zhen, W. Estimation of Grain Filling Rate and Thousand-Grain Weight of Winter Wheat Using Uav-Based Multispectral Image. Available at SSRN 4654298.